



Estimation and coordinated control for distributed parameter processes with a moving radiant actuator

Fan Zeng*, Beshah Ayalew

Clemson University, International Center for Automotive Research, 4 Research Drive, Greenville, 29607, United States

ARTICLE INFO

Article history:

Received 23 November 2009
Received in revised form 5 April 2010
Accepted 9 April 2010

Keywords:

Distributed estimation
Moving actuator
UV curing
Rule-based control
Coordinated control

ABSTRACT

This paper presents an estimation and control scheme for a class of industrial processes described by distributed parameter models with a moving radiant actuator. To overcome the lack of direct sensing alternatives for process state, a dual extended Kalman filter is established for estimating process status online based on a reduced process model and available output measurements. A distinct challenge that is addressed is the selection and construction of a suitable feedback signal from the distributed state estimate following the moving radiant actuator. The estimated status is then integrated into a rule-based feedback controller, which coordinates two manipulated variables of the moving radiant actuator to achieve the control objective. The two manipulated variables are the velocity and the radiant flux or power of the moving actuator. Both the estimation and feedback control strategies are demonstrated using computer simulations of one-dimensional distributed parameter models for an ultraviolet (UV) coating curing process involving a moving UV source. The results show that the proposed estimation and control schemes can significantly improve process quality and compensate for unknown disturbances on the target.

© 2010 Elsevier Ltd. All rights reserved.

1. Introduction

Many modern manufacturing processes involve the use of a moving actuator on a distributed parameter system. Examples can be found in various industrial applications that use robotic manipulators, such as painting, spray forming, welding, radiative drying and curing. The advantages of using a moving actuator in these processes include improved operating flexibility and reduced energy costs. Taking the automotive coating curing process as an example, the traditional convection-based approach requires a lot of energy to provide a high-temperature environment for curing the coating on a car body. Recent radiation-based curing technologies, such as ultraviolet (UV) curing, can use a radiative source attached to a robotic manipulator to complete the curing process near ambient temperatures [1,2]. These radiation-based processes can significantly reduce the energy consumption in the painting booths. Furthermore, there are also environmental benefits that could be associated with some of this alternative radiant source actuated processes. For example, successful radiative infrared (IR) drying of water-based paints could help avoid the need for volatile organic compounds (VOCs) as solvents [3,4].

Despite the above potential advantages, these radiation-based processes face various control related challenges. When using a moving radiant source/actuator, the trajectory of the manipulators should be carefully controlled since the relative orientation between the source and the target is paramount to the dynamics of the process and the quality of the end-product. In UV curing, for example, shadow effects need to be effectively accommodated when dealing with complex 3D geometries in order to obtain even cure on the target. Even for simple 2D targets and a source moving parallel to a target, the curing process should be controlled to compensate for disturbances that could arise from prior process defects or material property unevenness. Moreover, control challenges arise due to the fact that these radiant source actuated processes are distributed parameter processes with an actuator that moves in space. There are at least two issues with this. The first is lack of robust and cost-effective sensing alternatives for the distributed process state (e.g. cure conversion level) for use with a moving actuator in an industrial setting. The second is the selection or construction of suitable feedback signal that could be used to direct the moving actuator.

There is a volume of past and current research focused on developing optimal control strategies for distributed parameter systems [5–8] and implementing output feedback control through online measurements [9–13]. Early research in this area was conducted by Butkovskii in [5], which considers the formulation of the problem and the use of maximum principle for distributed parameter

* Corresponding author.

E-mail address: fzeng@clemson.edu (F. Zeng).

systems with mobile control sources. Approximate methods were provided to obtain solutions to these distributed optimal control problems [5]. Yeh and Tou expanded this research in [6], where they used methods such as successive Laplace transformations to reduce the complexity of solving the optimal control problems. However, the velocity of the moving actuator is set constant in their study. More recent research on the topic was conducted by Demetriou and co-workers [7,8]. They considered the problem as the optimal guidance and scheduling of the moving actuator within a set of pre-assigned admissible positions [7,8]. In their proposed control solution, both the position and control input of the actuator are optimally determined at each time interval. However, the practical actuation limitations and disturbances were not discussed in their studies. Huissoon et al. addressed a multi-variable control problem for a practical distributed parameter manufacturing process [9]. They developed a state-feedback controller to minimize the output error and reject disturbances based on a linear process model. Optimization on energy use was not discussed. Similar research was conducted for a spray deposition process by Jones et al. [10]. They designed a time-varying H_2 controller to regulate the temperature profile of the target by adjusting the spray rate based on temperature feedback obtained through an infrared camera. However, the speed of the spray gun was not controlled. Doumanidis and Fourligkas discussed the similar temperature profile control problem for a scan welding process in [11]. Both the motion and power of the torch were controlled in their study using 2D thermal imaging. The authors of the present paper have also done similar previous work in thermal-vision based feedback control in [12,13], but the estimation of distributed states and parameters and the coordination of multiple manipulated variables of the moving actuator were not considered and discussed.

Most of the methods described above require either predicting the process state by using a process model or measuring the output of the process through a transducer. Extensive work exists on the design and use of online estimators that combine both the predicting and sensing approaches for estimating the process state and use it for feedback control. The general methods for state and parameter estimation in chemical and biochemical processes are summarized in [14]. There, both the extended Luenberger and Kalman observers were introduced and the estimation methods for uncertain kinetic parameters associated with the state estimation were discussed. Soucy and Holt provide a framework for modeling, estimation and control of processing polymer composites in [15]. They proposed the method of using temperature measurement and an extended Kalman filter to estimate the extent of reaction and use the estimated state to monitor and control the process. In their study, the processing of the polymer composite was performed using fixed heaters. No moving heater/actuator was considered. VanAntwerp and coworkers [16] provided a review of estimation and control of cross-directional performance for sheet and film processes. Several methods used for estimating the cross-directional profile (of the sheet and film process) are introduced, such as time-varying Kalman filter, online imaging, etc. However, their discussion did not include the estimation of the profile in the machine-direction. Mobile distributed sensing technology was also used to estimate distributed parameter processes in [17]. There, two estimation-error driven guidance policies were developed to achieve improved estimation performance. While this study provides a solution to distributed state estimation, it requires direct measurement of the state by using these spatially distributed sensors.

Although these estimation methods described above have been widely used, the challenges, introduced by the moving actuator and the lack of direct state measurement for many distributed parameter processes, still need to be emphasized. In this work, we address the online estimation for distributed parameter processes with a moving radiant actuator and develop associated control strategies

that will use the estimated process state. The design of the online estimator involves a dual extended Kalman filter (DEKF) adopted to identify unknown distributed model parameters adaptively and improve the state estimation by using the updated model. The issue of feedback signal construction and selection is also addressed and then a rule-based feedback control strategy is adopted to coordinate two manipulated variables. The distributed parameter model of a 1D ultraviolet (UV) curing process with a moving source is used throughout this paper to illustrate the main points.

The rest of the paper is organized as follows. Section 2 describes a generalized 1D model of the distributed-parameter processes addressed here and also provides details for the UV curing process model that will be used in subsequent discussions. Section 3 addresses the design of the online estimator for both process state and model parameters. The coordinated feedback control strategy is detailed in Section 4. Section 5 presents and discusses the simulation results on the estimation and control performances for the UV curing example. Section 6 gives the conclusions of this work.

2. Problem formulation

2.1. A general 1D scanning problem

Many manipulator-based processes can be simplified as the 1D scanning problem illustrated in Fig. 1. A point source is used to indicate the moving actuator. u_a and v_a denote the input (mass or energy) and the scanning velocity of the actuator, respectively. u_t represents the amount of input transferred from the actuator to an arbitrary point of the target strip. The relationship between u_a (input at the actuator) and u_t (input at the target strip), which depends on the relative configuration between the actuator and target strip, can be described by the position vector \vec{d} and orientation angle θ . The two normal vectors with respect to actuator and target strip are denoted by \vec{n}_a and \vec{n}_t , respectively. The distance between the actuator path and target strip is denoted by d_0 .

The 1D scanning problem shown in Fig. 1 can be decomposed into three fundamental phases: transmission, reaction and co-evolution. The mathematical descriptions of these phases may be modeled by the following nonlinear functions:

$$u_t(x, t) = E[u_a(t), \vec{d}(x, t), \theta(x, t), \vec{p}_E] \quad (1)$$

$$\frac{d\vec{\omega}(x, t)}{dt} = R[\vec{\omega}(x, t), u_t(x, t), \vec{p}_R] \quad (2)$$

$$\frac{d\vec{\eta}(x, t)}{dt} = C[\vec{\eta}(x, t), \vec{\omega}(x, t), u_t(x, t), \vec{p}_C] \quad (3)$$

where E , R and C denote nonlinear functions representing transmission, reaction and co-evolution, respectively. t and x represent time and the position of an arbitrary point at the target strip, respectively. Eq. (1) describes the distribution of the input at the target strip (u_t), which varies with position and time. It is determined by a function of the input at the actuator (u_a), the position vector (\vec{d}),

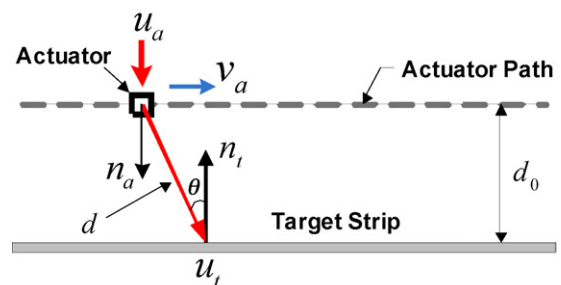


Fig. 1. The 1D scanning problem.

the orientation angle (θ), and a parameter vector (\vec{p}_E). In Eq. (2), $\vec{\omega}$ denotes the state vector describing key variables in the reaction phase of the process. The vector \vec{p}_R represents a set of parameters related to the reaction phase. The co-evolution phase is given by Eq. (3), in which $\vec{\eta}$ and \vec{p}_C denote the state and parameter vectors in this phase, respectively. In the following subsection, an ultraviolet (UV) curing process is used as an example to illustrate the above 1D scanning problem.

2.2. The UV curing process

The 1D scanning UV curing process includes the energy transmission from the UV radiator to the target, the photo-initiated polymerization within the target, and the associated thermal evolution. To model a basic UV curing process for thin films where variations along the film depth are neglected, the mathematical equations can be written as follows [18–21].

$$I(x, t) = k(x) \frac{\varphi(t) [\cos \theta(x, t)]^2}{\pi |\vec{d}(x, t)|^2} \quad (4)$$

$$\begin{cases} \frac{d[PI](x, t)}{dt} = -\phi \varepsilon [PI](x, t) I(x, t) \\ \frac{d[M](x, t)}{dt} = -\kappa \sqrt{\phi \varepsilon [M](x, t)} \sqrt{[PI](x, t) I(x, t)} \end{cases} \quad (5)$$

$$\frac{dT(x, t)}{dt} = \frac{1}{\rho c} \left\{ \nabla [\lambda \nabla T(x, t)] - \Delta H \frac{d[M](x, t)}{dt} - h [T(x, t) - T_\infty] \right\} \quad (6)$$

The variables and parameters used in Eqs. (4)–(6) are defined in Table 1. If the actuator’s position in Fig. 1 is denoted by x_a , then the position vector and orientation angle can be expressed by:

$$|\vec{d}(x, t)| = \sqrt{(x_a - x)^2 + d_0^2} = \sqrt{\left(\int_0^t v_a d\tau - x \right)^2 + d_0^2} \quad (7)$$

$$\cos \theta(x, t) = \frac{d_0}{|\vec{d}(x, t)|} = \frac{d_0}{\sqrt{\left(\int_0^t v_a d\tau - x \right)^2 + d_0^2}} \quad (8)$$

Table 1
Primary variables and parameters of the UV curing process model.

| Variables and parameters | Description |
|-----------------------------------|---|
| $I(x, t)$ | UV irradiance at the target (W/m^2) |
| $\vec{d}(x, t)$ | Position vector from the actuator to an arbitrary point of the target (m) |
| $\theta(x, t)$ | Orientation angle between the actuator and an arbitrary point of the target (rad) |
| $\varphi(t)$ | UV radiant power of the actuator (W) |
| $k(x)$ | Efficiency factor for UV absorption |
| $[PI](x, t)$ | Photo-initiator concentration (mol/L) |
| $[M](x, t)$ | Monomer concentration (mol/L) |
| ϕ | Quantum yield for initiation (mol/Einstein) |
| ε | Molar absorptivity (L/mol/m) |
| $\kappa (\kappa = k_p/k_t^{0.5})$ | Composite factor involving the propagation rate constant k_p and termination rate constant k_t ($(\text{L/mol/s})^{0.5}$) |
| $T(x, t)$ | The temperature of an arbitrary point of the target ($^\circ\text{C}$) |
| T_∞ | Ambient temperature ($^\circ\text{C}$) |
| ρ | Average density of the target (kg/m^3) |
| c | Average specific heat ($\text{J/kg/}^\circ\text{C}$) |
| λ | Average thermal conductivity ($\text{W/m/}^\circ\text{C}$) |
| ΔH | Polymerization enthalpy (J/mol) |
| h | Average convective heat transfer coefficient ($\text{W/m}^2/^\circ\text{C}$) |

Solving the first differential equation in Eq. (5), we have:

$$[PI](x, t) = [PI](x, t_0) \exp(-\phi \varepsilon \int_0^t I(x, \tau) d\tau) \quad (9)$$

Substituting Eqs. (7), (8) into (4), substituting Eq. (9) into the second differential equation in Eq. (5), and rearranging Eq. (6), we obtain:

$$I(x, t) = \frac{k(x) \varphi(t) d_0^2}{\pi \left[\left(\int_0^t v_a d\tau - x \right)^2 + d_0^2 \right]^2} \quad (10)$$

$$\begin{aligned} \frac{d[M](x, t)}{dt} &= -\kappa \sqrt{\phi \varepsilon [PI](x, t_0) [M](x, t)} \\ &\times \exp\left(-\frac{\phi \varepsilon}{2} \int_0^t I(x, \tau) d\tau\right) \sqrt{I(x, t)} \end{aligned} \quad (11)$$

$$\frac{dT(x, t)}{dt} = \frac{1}{\rho c} \nabla [\lambda \nabla T(x, t)] - \frac{\Delta H}{\rho c} \frac{d[M](x, t)}{dt} - \frac{h}{\rho c} [T(x, t) - T_\infty] \quad (12)$$

Given the UV curing process described through Eqs. (10)–(12), the control objective can be summarized as follows: the key distributed state of monomer concentration $[M](x, t)$ should be regulated to a desired level by adjusting the actuator’s inputs of UV radiant power φ and scanning velocity v_a . To achieve this control objective in the presence of disturbances, it is necessary to monitor the cure status in real time. However, the direct measurement of the key state (monomer concentration distribution) is difficult to achieve in industrial settings due to high equipment cost or inconvenient form factors of available instruments (e.g. FTIR, DSC, etc.) [22–24]. The alternative approach is to measure some other output of the process, such as the temperature distribution on the target obtained from thermal imaging, and estimate the monomer concentration indirectly. This issue will be discussed in detail in the next section.

3. Online state and parameter estimation

Two challenges can be identified in the estimation of the distributed process states while using a moving radiant actuator. First, since the process states and uncertain parameters are spatially distributed, the estimation is generally computationally intensive. This can be addressed to some extent by using a reduced or simplified model for the process. Second, with moving actuators, the observability depends on the actuator’s motion and location. This changing observability will have a significant effect on the estimation performance.

In this section, the dual extended Kalman filter (DEKF) [25,26] will be used to achieve combined state and parameter estimation in consideration of these two challenges. For the present class of 1D scanning problems described in Section 2.1, the fundamental architecture of the DEKF estimator adopted for this work is depicted in Fig. 2.

Here, $u_a(t)$ and $v_a(t)$ denote the two input variables at the actuator, respectively. $\vec{\eta}(x, t)$ represents the state vector of the co-evolution phase, and here it is taken as the measurable output of the process. The DEKF estimator then uses the process model and these input and output measurements to estimate the parameter and state vectors. The parameter vector \vec{p} is composed of some unknown parameters of interest for the transmission, reaction and co-evolution phases. The state vector usually denotes the state of the reaction phase $\vec{\omega}(x, t)$ which is difficult to measure directly.

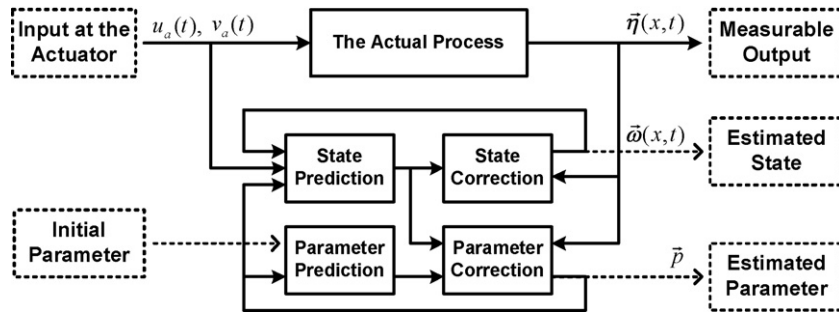


Fig. 2. The basic architecture of the DEKF estimator.

The following paragraphs detail the implementation of this DEKF estimator to the UV curing example.

3.1. Simplified numerical model

To design the DEKF estimator, a simplified numerical model consisting of the main nonlinearities of the process should be developed first. The continuous target strip in Fig. 1 is replaced with a discrete one composed of a number of units along the strip. Similar discretization is applied in the time domain. Since the average thermal conductivity along the target strip is usually very small, the heat conduction term in Eq. (12) can be ignored, which reduces Eq. (12) to a local ordinary differential equation. In addition, the initial photo-initiator and monomer concentrations for all units along the target strip are assumed to be the same.

Given the above discretization and simplifications, the original curing process model described by Eqs. (10)–(12) can be represented in the following discrete form:

$$I(i, j) = \frac{k(i)\varphi(j)d_0^2}{\pi \left[\left(\sum_{n=0}^j v_a(n)\Delta t - i\Delta x \right)^2 + d_0^2 \right]^2} \quad (13)$$

$$[M](i, j) = \left[-\kappa \sqrt{\phi \varepsilon [PI]_0} \exp \left(-\frac{\phi \varepsilon}{2} \sum_{n=0}^j I(i, n)\Delta t \right) \sqrt{I(i, j)\Delta t + 1} \right] \times [M](i, j-1) \quad (14)$$

$$T(i, j) = -\frac{\Delta H}{\rho c} \{ [M](i, j) - [M](i, j-1) \} - \left(\frac{h}{\rho c} \Delta t + 1 \right) T(i, j-1) + \frac{h}{\rho c} \Delta t T_\infty \quad (15)$$

$$[M](i, 0) = [M]_0, \quad [PI](i, 0) = [PI]_0, \quad T(i, 0) = T_\infty \quad (16)$$

$$i = 0, 1, 2, \dots, Q; \quad j = 0, 1, 2, \dots, N. \quad (17)$$

Here, the indexes j and i denote the j th time step and the i th unit from the left-end of the target strip, respectively. Q and N represent the total number of strip units and time intervals. Δx and Δt are the lengths of spatial and temporal steps. $[M]_0$ and $[PI]_0$ are initial monomer and photo-initiator concentrations for all units along the strip. Assuming that the photo-initiated curing (monomer consumption) is rapid and occurs before any significant diffusion of monomer takes place, the evolution of monomer concentration on each unit can be decoupled from those of the adjacent units. In addition, considering a substrate and film with much lower thermal conductivity compared to the exothermic polymerization, it is possible to ignore the diffusion term in the thermal dynamic equation. Then, the temperature on each unit is also decoupled from those

of the adjacent units. These two assumptions give model reduction that allows us to design the DEKF observer for each unit independently. The assumptions are verified later when the estimators are applied to the full nonlinear model.

There are two types of parameters associated with the curing process: constant unknown parameters and spatially distributed unknown parameters. The first type includes the chemical parameters (κ , ϕ , ε , and ΔH), material-related parameters (ρ and c), and the heat transfer coefficients (h). These parameters are usually obtained through off-line measurement or estimation. Compared to the constant unknown parameters, the spatially distributed ones can only be estimated online. The distributed efficiency factor k is an example of these parameters. The distribution of this parameter may be influenced by material property variation or paint unevenness on the target strip. In addition, the distribution of k also varies with target types and configurations. To ensure the essential accuracy of the model used for state estimation and feedback control, online identification of the distribution of the efficiency factor is also included in the development of the observer.

3.2. Development of the DEKF

Given the high nonlinearity of the curing process described by Eqs. (13)–(15), the dual extended Kalman filter (DEKF) will be used to design the state estimator. Since the heat conduction term has been neglected in the simplified model, the estimation for each unit of the target strip can be performed independently. This simplification makes it possible to break a single large-scale DEKF into a series of independent local DEKFs. This reduces the complexity of the design process. Considering an arbitrary unit of the target strip, the state-space form of the curing process dynamics can be represented by:

$$\begin{aligned} \mathbf{x}(i, j) &= F[\mathbf{x}(i, j-1), \mathbf{u}(i, j-1), \mathbf{p}] + \mathbf{n}_s(i, j-1) \\ \mathbf{y}(i, j) &= C\mathbf{x}(i, j) + \mathbf{n}_m(i, j) \end{aligned} \quad (18)$$

Here, F represents a highly nonlinear function combining Eqs. (13)–(15). \mathbf{x} , \mathbf{u} , and \mathbf{p} denote the state, input and parameter vectors, respectively. The three vectors are defined by:

$$\mathbf{x} = [[M], T]^T, \quad \mathbf{u} = [\varphi, v_a]^T, \quad \mathbf{p} = [k, \kappa, \phi, \varepsilon, \rho, c, h]^T \quad (19)$$

The output vector $\mathbf{y}(i, j)$ has only one component, which is the temperature T measured through thermal imaging. Therefore, the observation matrix C is set to $[0, 1]$. The vectors \mathbf{n}_s and \mathbf{n}_m represent the system and measurement noises which are assumed to be white and with normal probability distributions. The state and parameter estimation scheme can be designed in the following manner.

3.2.1. The dual EKF structure

In the discretization, each unit of the target strip has its own value of efficiency factor k . The first EKF is used to estimate the value of k adaptively starting from an initial value. The second EKF then uses the noise-free model (with updated k) and the temperature

measurement to estimate the key state (monomer concentration) of the curing process.

3.2.2. The estimation procedure

The implementation of the above Dual EKF structure follows a recursive procedure involving two fundamental steps (prediction and correction) to get an optimal estimation of both the state and parameters. The following formulation, which is adopted from existing literature on Kalman filtering [25,26], outlines the estimation procedures.

Parameter prediction :

$$\hat{k}^-(i, j) = \hat{k}(i, j - 1), \quad p = [\hat{k}^-(i, j), \kappa, \phi, \varepsilon, \rho, c, h]^T \quad (20)$$

$$\text{State prediction : } \hat{x}^-(i, j) = F[\hat{x}(i, j - 1), u(i, j - 1), p] \quad (21)$$

$$\text{State correction : } \hat{x}(i, j) = \hat{x}^-(i, j) + K_s[y(i, j) - C\hat{x}^-(i, j)] \quad (22)$$

$$\text{Parameter correction : } \hat{k}(i, j) = \hat{k}^-(i, j) + K_p[y(i, j) - C\hat{x}^-(i, j)] \quad (23)$$

In Eqs. (20) and (21), $\hat{k}^-(i, j)$ and $\hat{k}(i, j - 1)$ are the prediction of k at time j and the previous estimate of k at time $j - 1$. Similarly, $\hat{x}^-(i, j)$ and $\hat{x}(i, j - 1)$ represent the prediction and previous estimate of the state vector x at time j and $j - 1$, respectively. In the prediction step, both the parameter and state vectors are updated by using the estimation results of the last time step and the process model. Then the final estimation is completed after the predicted parameters and states are corrected based on the current measurement. The two gain matrices (K_s and K_p) are calculated in an optimal manner to minimize the estimated error covariance. They are also updated with time by using the following recursive equations [25,26]:

$$\begin{aligned} \text{For } K_s : \hat{P}_s^-(j) &= \Phi \hat{P}_s(j - 1) \Phi^T + Q, \\ K_s(j) &= \hat{P}_s^-(j) C^T [C \hat{P}_s^-(j) C^T + R]^{-1} \\ \hat{P}_s(j) &= [I - K_s(j) C] \hat{P}_s^-(j) \end{aligned} \quad (24)$$

$$\begin{aligned} \text{For } K_p : \hat{P}_p^-(j) &= \hat{P}_p(j - 1), \\ K_p(j) &= \hat{P}_p^-(j) H^T [H \hat{P}_p^-(j) H^T + R]^{-1} \\ \hat{P}_p(j) &= [I - K_p(j) H] \hat{P}_p^-(j) \end{aligned} \quad (25)$$

Here, P_s and P_p are the estimated error covariance matrices for state and parameter vectors, respectively. Q and R are constant covariance matrices for system and measurement noises. Since the only output of the system is the temperature in this case, the observation matrix C is set to $[0, 1]$. Φ and H are two Jacobian matrices defined as follows:

$$\Phi = \frac{\partial F}{\partial x} [\hat{x}(i, j - 1), u(i, j - 1), p] \quad (26)$$

$$H = C \frac{\partial F}{\partial k} [\hat{x}(i, j - 1), u(i, j - 1), p] \quad (27)$$

The matrices Φ and H need to be updated at each time step due to the high nonlinearity of the curing process. This requires a lot of computation. The ideal implementation of the above structure is to design a full-dimension estimator which has the same number of DEKFs as the number of target strip units. This increases the computation requirements even more. Therefore, it is desirable to reduce the dimension of the estimator to some reasonable level that is acceptable for both estimation accuracy and computational cost. In the present example, every other two successive units are assigned an estimator to approximate the monomer concentration

and efficiency factor for one of them, and the estimation for other intermediate units are obtained through interpolation.

4. Control strategy development

As outlined in the previous section, online estimation of the key state and unknown distributed parameters provides information about the current state of the process. This can then be used to develop a closed-loop control strategy and improve process performance and product quality. The design of a closed-loop control strategy for distributed parameter processes with moving radiant actuators poses at least two new challenges. First, the fact that the actuator has to move around to complete the process means that the feedback signal should emphasize local state distributions and should be selected in a manner that follows and/or guides the moving actuator. Second, these processes are usually influenced by multiple comparably dominant manipulated variables associated with the moving actuator; namely, its radiant power and velocity. The coordination between these control variables should be carefully considered. Taking the above two issues into account, a rule-based coordinated feedback control strategy is proposed for these 1D scanning problems. The control structure is illustrated in Fig. 3.

In Fig. 3, the desired process quality level q_d and the measurable state vector $\vec{\eta}(x, t)$ for the co-evolution phase are taken as the input and output, respectively, of the feedback control system. The estimated state vector ($\hat{\omega}(x, t)$) for the reaction phase is sent to the feedback signal generator to calculate the actual process quality level $q(t)$. The rule-based controller then uses the error signal $e(t)$ and some designed rules to coordinate the two manipulated variables $u_a(t)$ and $v_a(t)$ of the actuator. The implementation of this closed-loop control strategy to the UV curing process will be discussed below.

4.1. Local feedback signal generation

For closed-loop control of the curing process, a feedback signal needs to be generated first. Although the online state and parameter estimation can provide complete information for the whole target, only part of this information can be used when the actuator is passing by any position of the target strip. This is because the dominant polymerization normally occurs around the current position of the actuator. The feedback signal should then be generated within a defined sampling window around the location of the actuator. The size of this sampling window is defined by the number of units included in it, and its position is taken as the position of the unit in the middle of the window. The choices of the two parameters (sampling window size and position) have significant influences on the feedback signal.

The size of the sampling window mainly influences the precision of the feedback signal. Since the feedback signal is defined by the average monomer concentration of the units within the sampling window, a larger window usually gives a higher precision. However, it decreases the sensitivity for interference detection at the same time (e.g. discontinuities or jumps from defects). Therefore,

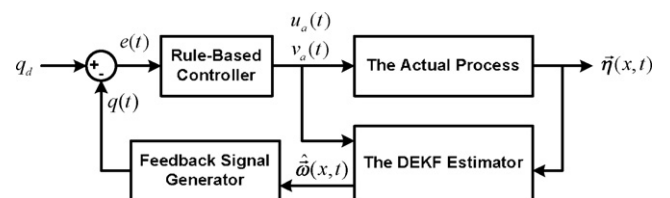


Fig. 3. The rule-based feedback control structure.

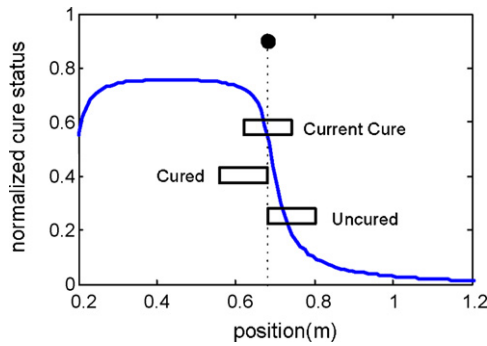


Fig. 4. The selection of the sampling window (the solid ball represents the moving actuator).

there is a trade-off between precision and sensitivity that must be considered when determining the size of the sampling window.

The position of the sampling window determines the accuracy of the feedback signal. It is natural to select the position of the sampling window as the one which is consistent with the current position of the actuator, since this is the area currently being cured. The alternative approaches involve shifted selections. The shift can be made either to past (bias to cured areas) or future (bias to uncured areas) directions along the path of actuator on the target strip. Here, the three selections, simply named as “current cure”, “cured” and “uncured”, are illustrated in Fig. 4.

In the curing process, all the three windows shown in Fig. 4 will simultaneously move along with the actuator. Obviously, the “cured” window has the highest cure conversion level, while the “uncured” one has the lowest level. The final feedback signal should be generated through a combination of the three. Such a formulation of the feedback signal is given by:

$$\alpha(j) = \sum_{u=1}^3 \left(\lambda_u \sum_{v=v_0}^{v_0+Z_u} \frac{[M]_0 - [M](v, j)}{[M]_0} \right) \tag{28}$$

$$v_0 = i + \frac{u-3}{2} Z_u, \quad \lambda_u \in [0, 1], \quad \sum_{u=1}^3 \lambda_u = 1$$

In Eq. (28), $\alpha(j)$ denotes the feedback signal at the time j . The subscription u is the index of the three windows ($u = 1, 2, 3$ corresponding to “cured”, “current cure” and “uncured”). λ_u is the weight coefficient for each window. Z_u represents the size of the sampling window and is equal to the number of target strip units included in each window. i denotes the index of the unit right under the actuator’s current position. $[M]_0$ represents the initial monomer concentration.

4.2. Coordinated control design

The main control objective for the curing process is to achieve the desired cure conversion level by adjusting the radiant power (φ) and scanning velocity (v_a) of the actuator. Since this is a multiple-input single-output (MISO) problem in which the monomer concentration distribution is controlled by the radiant power and scanning velocity, the control strategy needs to coordinate the use of the two manipulated variables. Here, some open-loop calibrations were conducted to investigate the influence of the two variables on the curing process and select the nominal values for them. Then, a rule-based PID controller is designed to close the loop and achieve the control objective.

4.2.1. Open-loop calibration

The open-loop calibration is done using a simulation model of the above curing process. Due to the high nonlinearity of the system model, explicit influences of the two manipulated variables (φ, v_a) on the process state are difficult to obtain analytically. Therefore, a few model simulation tests have been done to determine the influences of different combinations of the two variables on the curing process by generating the two maps (2D and 3D) illustrated in Fig. 5.

It can be observed from Fig. 5 that a high scanning velocity requires associated high radiant power to achieve the same cure conversion level. Many combinations of radiant power and scanning velocity can potentially give the same desired cure conversion level. In this work, the selection of the two variables is made considering two major factors: the energy consumption and productivity. A static optimization can be used to select the nominal radiant power and scanning velocity. The corresponding cost function is described by:

$$\min J(v_a, \varphi) = \frac{1}{2} m v_a^2 + \varphi \frac{L}{v_a}, \quad \text{s.t. } f(v_a, \varphi) = \alpha_d, \tag{29}$$

$$v_0 \leq v_a \leq v_m, \quad 0 \leq \varphi \leq \varphi_m$$

Here, m and L denote the mass of the actuator and the length of the target strip, respectively. The constraint equation f describes the relationship of the two control variables for a specified cure conversion level α_d . The lower velocity limit v_0 represents the minimal scanning velocity to reach the required productivity. v_m and φ_m are the highest scanning velocity and maximum radiant power of the actuator, respectively. In practice, an approximation of the optimal combination can be obtained given the cure conversion level maps illustrated above and/or engineering experience with the process.

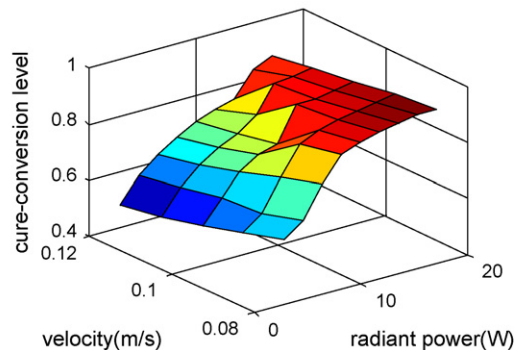
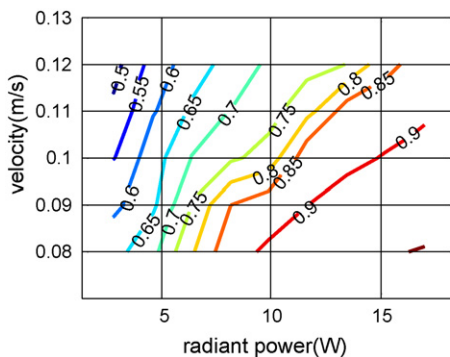


Fig. 5. Cure conversion level maps for different combinations of the radiant power and scanning velocity in the open-loop calibration.

4.2.2. Rule-based coordinated PID controller

Given the prevailing structure of two manipulated variables and construction of a single (per unit) feedback variable, it is necessary to have a combination or coordination scheme for manipulating these variables. The approach adopted here is to implement PID control loops based on some designed coordination rules [27–29]. A one-dimensional rule-based strategy, where only cure conversion level error is considered, is detailed here. The designed rules are shown in Table 2.

In Table 2, the range of the absolute value of the error is divided into three zones: $[0, c_1]$, $(c_1, c_2]$ and $(c_2, |e|_m]$, where $|e|_m$ is the maximum value of $|e|$. The desired and actual cure conversion levels are denoted by α_d and α . The latter is calculated by using Eq. (28). The nominal value of the velocity and radiant power of the actuator are denoted by v_{a0} and φ_0 , respectively. The weight coefficients assigned to the “cured”, “current cure” and “uncured” sampling windows are set to 1/6, 2/3, and 1/6 when the actuator stays at the starting position. Once the actuator begins to move, the weight coefficients are changed to 2/3, 1/6 and 1/6. When $|e|$ is located in the zone $(c_2, |e|_m]$, for example, at the beginning the curing process, the actuator stays at its original position and apply the maximum radiant power to reduce the error quickly. After the error has been brought to the zone $(c_1, c_2]$, the radiant power is cut to the half of its maximum value and the actuator begins to move. At the same time, a simple P controller is used to adjust the scanning velocity during this transition stage. Once the error further goes to the zone $[0, c_1]$, the velocity controller is replaced by two individual loops: a new PID controller for controlling the velocity and an additional P controller that controls the radiant power.

These rules are extracted from some basic understanding of the curing process. For example, near the starting point, the state error is large, and the radiant actuator has to stay at the starting point and apply the maximum power for a while before it moves away; otherwise the area around the starting point will suffer incomplete cure. Second, the actuator should move in advance once these areas around the starting point are close to fully cured, and the radiant power should be reduced accordingly to avoid over cure. A simple practical way to do this is to reduce the power to half of its maximum value and use a proportional controller to adjust the velocity during the transition. Once the state error falls into the desired range with the actuator moving, a PID controller is used to adjust the velocity and a proportional controller is used to regulate the radiant power.

It should be stated that, although these rules were easy to select and verify, and some optimality consideration has been made for the open-loop optimization calibration maps, the closed-loop control of the process with the moving actuator using the above rules is not necessarily optimal. To achieve a better implementation of closed-loop optimal coordination, a model predictive control (MPC) framework is currently being investigated by the authors. An added attraction of the framework, in addition to opti-

mality, is the possibility of including state and input constraints explicitly in the multi-variable coordination of the manipulated variables.

5. Results and discussion

In this section, simulation results will be presented to demonstrate the online estimation scheme and feedback control strategy outlined above with the 1D curing process as an example. The process simulation is performed using the full model described in Eqs. (4)–(6), and the estimator is developed using the simplified model characterized by Eqs. (13)–(15). Most of the chemical, thermal and material parameters used in this simulation are obtained from the references [20,21]. The length of the target strip is set to 1.4 m and the perpendicular distance between the actuator and the target strip is set to 0.03 m.

5.1. Estimator performance

To test the performance of the online state and parameter estimation strategy with the DEKF, a scenario with constant scanning velocity and radiant power is considered. The main parameters used in this analysis are shown in Table 3. The estimator is tuned by adjusting the covariance matrices Q and R . The actuator scans the target strip only within the range $[0.2, 1.2](m)$. Edge effects are not addressed. The corresponding results are given in Figs. 6–9.

In Figs. 6 and 7, the moving actuator is represented by a solid ball. The results in Fig. 6 show that the estimated cure conversion level matches the actual value well. In Fig. 7, the estimation of the efficiency factor distribution is gradually improved and completed as the actuator moves from the left to the right end. When the actuator passes the middle of the target, for those units that have not been cured yet, the estimated efficiency factors are hardly consistent with the actual values until the actuator approaches those units. This is because the corresponding observability of parameter estimation is poor for those units that are far away from the moving actuator. A derivation and discussion of the observability of the system is included in the appendix of the paper.

The time history of the error dynamics for both state and parameter estimation is given by Figs. 8 and 9, respectively. The confidence region is given by the plus and minus 3 standard deviations of the error covariance for both the state and parameter estimation. In Fig. 8, the state estimate errors at $x = 0.4 m$ (left) and $x = 0.7 m$ (right) begin to converge around $t = 2 s$ and $t = 5 s$, which are the moments when the actuator moves across the two positions. Similar convergence can be found in the parameter estimate errors shown in Fig. 9. These results demonstrate the inherent characteristic of the class of problems addressed in this paper: that the performance of the state and parameter estimators is significantly influenced by the changing observability following the actuator's movement.

Table 2 The control coordination rules.

| Error ($e = \alpha_d - \alpha$) | Control rules |
|-----------------------------------|---|
| $c_2 < e \leq e _m$ | $v_a = 0, \quad \varphi = \varphi_m$ (usually applied at the beginning of the curing process) |
| $c_1 < e \leq c_2$ | $v_a = v_{a0} - K_{p1}e, \quad \varphi = \frac{1}{2}\varphi_m$ (applied during the transition stage) |
| $ e \leq c_1$ | $v_a = v_{a0} - (K_{pv}e + K_{iv} \int edt + K_{dt}\dot{e})$ $\varphi = \varphi_0 + K_{p\varphi}e$ (applied during the steady stage) |

Table 3 The selected parameters for estimator performance analysis.

| Parameters | Values |
|--|--|
| Scanning velocity | $v_a = 0.1 m/s$ |
| Radiant power | $\varphi = 10.2 W$ |
| Efficiency factor (for the actual model) | $k(x) = -2x/7 + 0.8, x \in [0, 1.4] (m)$ |
| Initial value for k estimation | $\hat{k}(x)_0 = 0.2, x \in [0, 1.4] (m)$ |
| System noise | $E[\mathbf{n}_s] = [0, 0]^T, \quad Var[\mathbf{n}_s] = [1, 1 \times 10^{-4}]^T$, Units of \mathbf{n}_s : [mol/L, °C] ^T |
| Measurement noise | $E[\mathbf{n}_m] = 0, \quad Var[\mathbf{n}_m] = 1 \times 10^{-6}$, Units of \mathbf{n}_m : °C |

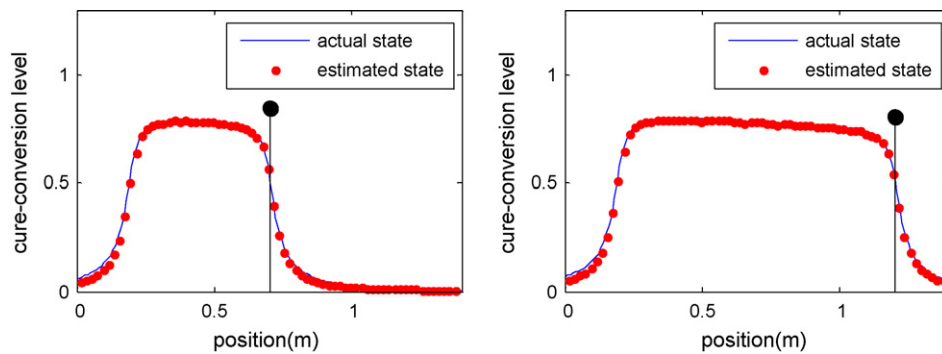


Fig. 6. The actual and estimated state distribution with the moving actuator at the middle (left) and at the end (right). The solid ball represents the moving actuator.

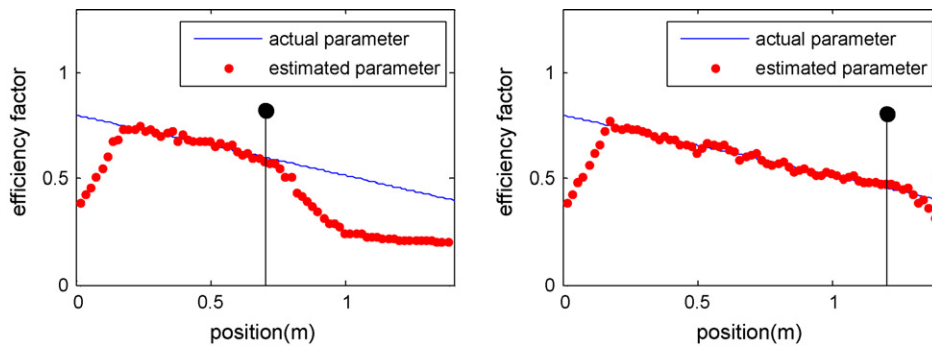


Fig. 7. The actual and estimated parameter distribution with the moving actuator at the middle (left) and at the end (right). The solid ball represents the moving actuator.

5.2. Demonstration of the feedback control strategy

It can be seen from Fig. 6 that the open-loop curing cannot ensure the uniformity along the target with the existence of some disturbances, such as the uneven distribution of the efficiency

factors (it decreases with x as shown in Fig. 7). Thus, the cure conversion level distribution in Fig. 6 shows a similar gradient. On the other hand, the closed-loop approach can monitor the online cure status through measurement and estimation, and adjust the manipulated variables to compensate for these disturbances. In this

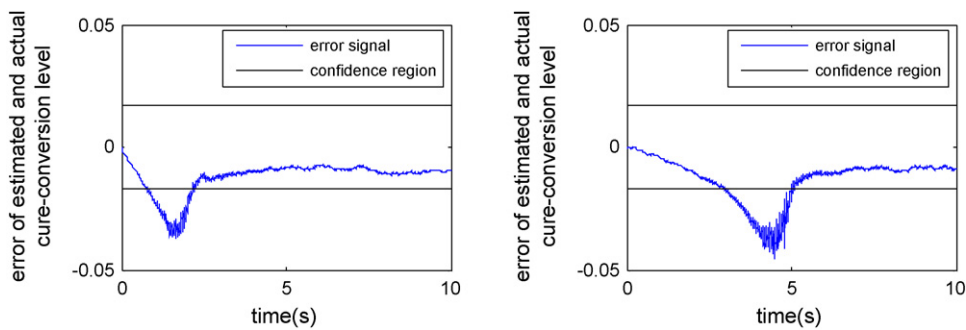


Fig. 8. The time history of the error of estimated and actual cure conversion level at two positions: $x=0.4$ m (left) and $x=0.7$ m (right).

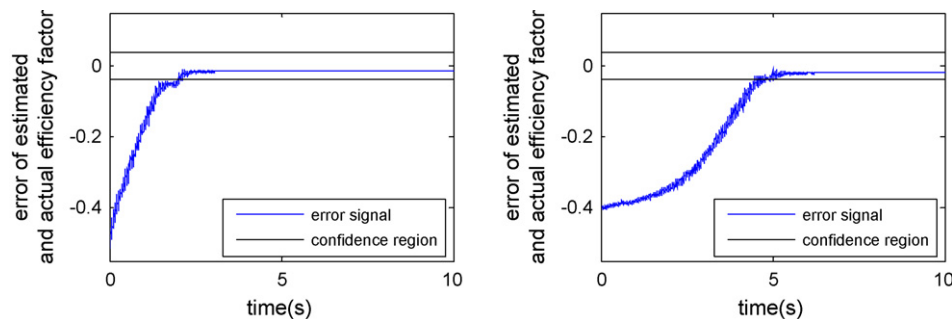


Fig. 9. The time history of the error of estimated and actual efficiency factor at two positions: $x=0.4$ m (left) and $x=0.7$ m (right).

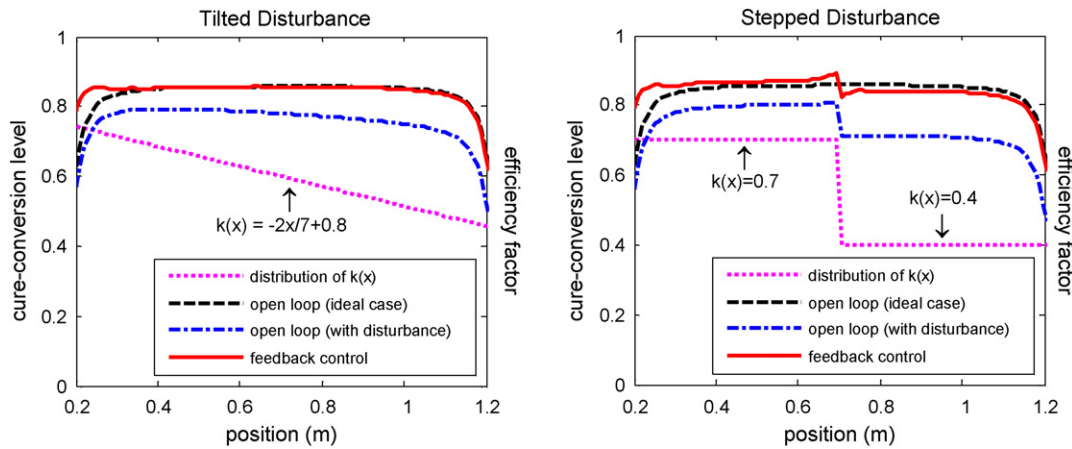


Fig. 10. The cure conversion level distribution for the scenarios of tilted (left) and stepped (right) disturbances in the efficiency factor k .

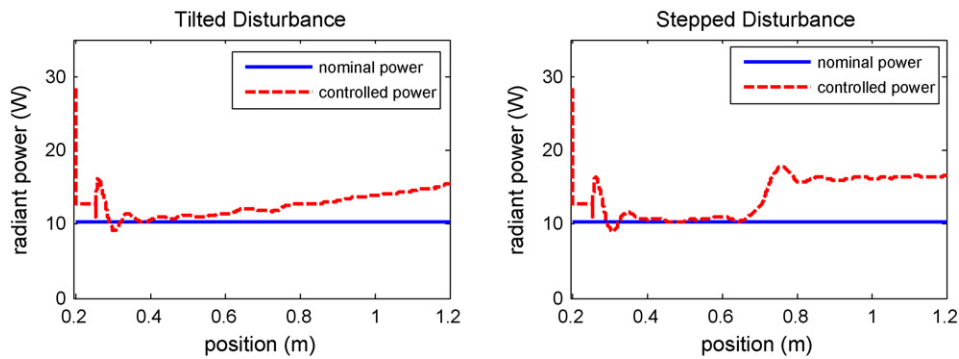


Fig. 11. The radiant power distribution for the scenarios of tilted (left) and stepped (right) disturbances in the efficiency factor k .

subsection, the proposed rule-based coordinated feedback control strategy will be demonstrated considering two different disturbance scenarios. One of them deals with the tilted distribution of the efficiency factors shown in Fig. 7. The other considers a stepped distribution ($k(x) = 0.7, 0 \leq x < 0.7 \text{ m}; k(x) = 0.4, 0.7 \text{ m} \leq x \leq 1.4 \text{ m}$). The corresponding results are shown in Figs. 10–13.

Fig. 10 illustrates the cure conversion level distributions considering three different control cases for the two scenarios (with tilted and stepped disturbances in the efficiency factor k). The desired cure conversion level is set to 0.85. If no disturbance exists (the efficiency factor $k(x) = 1$ everywhere), the open-loop method can achieve good cure uniformity by using the optimal radiant power and scanning velocity obtained from Eq. (29). However, the tilted and stepped disturbances in the efficiency factor distribution will cause cure unevenness (illustrated by the dash-dot lines in Fig. 10)

when the same configuration is implemented in the actual curing process. Compared to the open-loop curing method, the closed-loop approach can achieve the desired cure conversion level and give acceptable cure uniformity for both the tilted and stepped scenarios, although a slight unevenness is found around the step position for the stepped distance scenario.

Fig. 11 shows the radiant power distributions when the actuator is at different positions. For both the tilted and stepped scenarios, the radiant power is first regulated to the nominal value based on the control rules in Table 2. Then, it is adaptively adjusted for different types of disturbances, corresponding to the radiance power increasing in tilted and stepped manners, respectively. Fig. 12 illustrates the simultaneous/coordinated scanning velocity distributions for the two cases. Although the nominal value is set to 0.1 m/s, the scanning velocity for both the tilted and stepped sce-

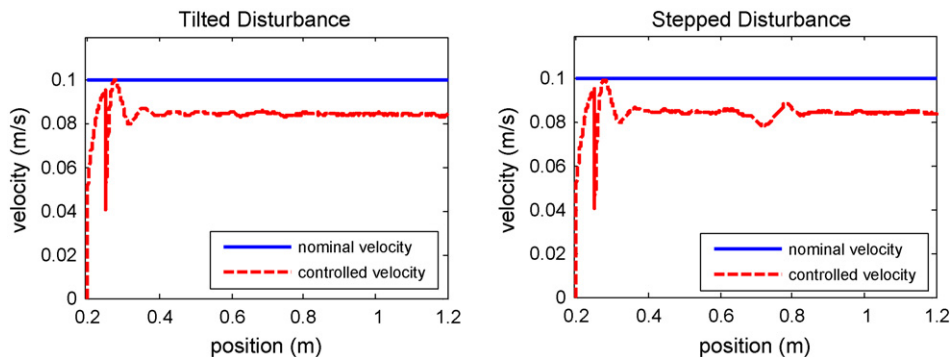


Fig. 12. The scanning velocity distributions for the scenarios of tilted (left) and stepped (right) disturbances in the efficiency factor k .

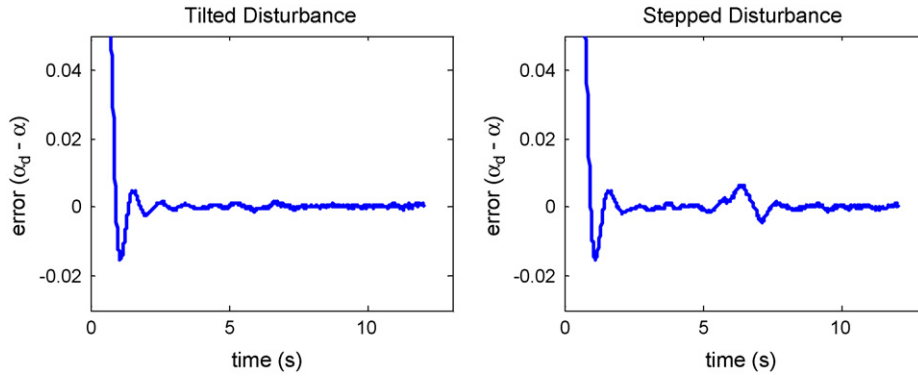


Fig. 13. The error dynamics for the scenarios of tilted (left) and stepped (right) disturbances in the efficiency factor k .

narios is automatically pulled to a lower level to compensate for the variation of efficiency factor from 1 (the ideal value). Comparing Figs. 11 and 12, one observes that the unevenness of efficiency factor is mainly counteracted by the control of the radiant power, and the control of scanning velocity contributes more to ensure the desired cure conversion level. The error dynamics shown in Fig. 13 indicates that the error between the desired and actual cure conversion level settles within 1.5 s for both the tilted and stepped scenarios. It is of course possible to tune these behaviors by adjusting the control gains and rule-thresholds defined in Table 2.

The above results demonstrate that the proposed closed-loop control of the curing process can significantly improve the cure quality over what can be obtained in open-loop control in the presence of disturbances by effectively coordinating the radiant power and actuator velocity with carefully designed rules.

6. Conclusion

This paper presented a framework of estimation and control for distributed parameter processes that employ a moving radiant actuator. The proposed estimation and control schemes were described in detail for a 1D scanning UV curing process, for which an effective online state and parameter estimator was designed based on a simplified process model with unknown distributed parameters. A dual extended Kalman filtering structure was implemented to update the estimations of both the distributed state and parameter in parallel. Using the estimated process state, a feedback control strategy was developed to enhance the process quality through rule-based coordination of two manipulated variables: actuator velocity and radiant power. Both the proposed estimator and controller have been applied in the simulation of the complete nonlinear model of a 1D UV curing process with a moving radiant actuator/UV source. The results showed that the online estimation scheme provides a good estimation of the actual process state in the presence of system and measurement noises, and the rule-based coordinated feedback control strategy can succeed in improving process quality by effectively compensating for disturbances such as variations in absorption efficiencies.

The presented framework highlighted some major issues that have yet to be addressed for the distributed parameter processes employing a moving radiant actuator. These include: (1) construction and selection of a suitable feedback signal for use with a moving actuator on a distributed domain, (2) a formal treatment of the estimation challenges due to the dependence of the observability distribution on the position of the actuator, (3) incorporation of advanced optimal coordination strategies (e.g. Model Predictive Control) to achieve online optimization of the actuator's trajectory and radiant power for further improvement of process control. These issues will be investigated further in future work.

Appendix A. Observability analysis

A.1. Further simplification of the curing process model

Equations (Eqs. (13)–(15) in the paper) that describe the curing process can further be simplified as follows:

$$I(i, j) = k(i)\Upsilon(i, j) \quad (\text{A1})$$

$$[M](i, j) = \left\{ \eta_1 \exp \left[\eta_2 k(i) \sum_{n=0}^j \Upsilon(i, n) \Delta t \right] [k(i)\Upsilon(i, j)]^{0.5} \Delta t + 1 \right\} \times [M](i, j - 1) \quad (\text{A2})$$

$$T(i, j) = \eta_3 \{ [M](i, j) - [M](i, j - 1) \} + \eta_4 T(i, j - 1) + \eta_5 \quad (\text{A3})$$

where

$$\Upsilon(i, j) = \frac{\varphi(j)d_0^2}{\pi \left[\left(\sum_{n=0}^j v_a(n) \Delta t - i \Delta x \right)^2 + d_0^2 \right]^2} \quad (\text{A4})$$

$$\eta_1 = -\kappa \sqrt{\phi \varepsilon [PI]_0}, \quad \eta_2 = -\frac{\phi \varepsilon}{2}, \quad \eta_3 = -\frac{\Delta H}{\rho c},$$

$$\eta_4 = -\left(\frac{h}{\rho c} \Delta t + 1 \right), \quad \eta_5 = \frac{h}{\rho c} \Delta t T_\infty \quad (\text{A5})$$

From Eq. (A2), we obtain:

$$[M](i, j) - [M](i, j - 1) = \eta_1 \exp \left[\eta_2 k(i) \sum_{n=0}^j \Upsilon(i, n) \Delta t \right] \times [k(i)\Upsilon(i, j)]^{0.5} \Delta t [M](i, j - 1) \quad (\text{A6})$$

Substituting Eq. (A6) into (A3) yields:

$$T(i, j) = \eta_3 \eta_1 \exp \left[\eta_2 k(i) \sum_{n=0}^j \Upsilon(i, n) \Delta t \right] \times [k(i)\Upsilon(i, j)]^{0.5} \Delta t [M](i, j - 1) + \eta_4 T(i, j - 1) + \eta_5 \quad (\text{A7})$$

Combining Eqs. (A2) and (A7), the curing process model can be represented in the following form:

$$[M](i, j) = f_1 = [\eta_1 \Psi(i, j) + 1] [M](i, j - 1)$$

$$T(i, j) = f_2 = \eta_3 \eta_1 \Psi(i, j) [M](i, j - 1) + \eta_4 T(i, j - 1) + \eta_5 \quad (\text{A8})$$

where

$$\Psi(i, j) = \exp \left[\eta_2 k(i) \sum_{n=0}^j \Upsilon(i, n) \Delta t \right] [k(i) \Upsilon(i, j)]^{0.5} \Delta t \quad (\text{A9})$$

The measurement equation of the system is denoted by:

$$y(i, j) = \begin{bmatrix} 0 & 1 \end{bmatrix} \begin{bmatrix} [M](i, j) \\ T(i, j) \end{bmatrix} \quad (\text{A10})$$

A.2. Observability analysis for the state estimator

For those units (along the strip) which are far away from the moving source, the received irradiance ($I(i, j) = k(i) \Upsilon(i, j)$) is very small. Therefore, the term $\Psi(i, j)$, which is a function of the irradiation, is almost equal to zero. Then, the Jacobian matrix of Eq. (A8) can be calculated as:

$$\begin{bmatrix} \frac{\partial f_1}{\partial [M]} & \frac{\partial f_1}{\partial T} \\ \frac{\partial f_2}{\partial [M]} & \frac{\partial f_2}{\partial T} \end{bmatrix} = \begin{bmatrix} \eta_1 \Psi(i, j) + 1 & 0 \\ \eta_3 \eta_1 \Psi(i, j) & \eta_4 \end{bmatrix} \approx \begin{bmatrix} 1 & 0 \\ 0 & \eta_4 \end{bmatrix} \quad (\text{A11})$$

Now we can check the observability matrix:

$$C = \begin{bmatrix} 0 & 1 \end{bmatrix}, \quad A = \begin{bmatrix} 1 & 0 \\ 0 & \eta_4 \end{bmatrix}, \quad \begin{bmatrix} C \\ CA \end{bmatrix} = \begin{bmatrix} 0 & 1 \\ 0 & \eta_4 \end{bmatrix} \quad (\text{A12})$$

The rank of the observability matrix is less than two, which means the states are not fully observable for those units which are far away from the moving source.

A.3. Observability analysis for the parameter estimator

To discuss the observability for the parameter estimator, the following equations will be considered.

$$k(i, j) = k(i, j - 1) \quad (\text{A13})$$

$$T(i, j) = f_3 = \eta_3 \eta_1 \exp \left[\eta_2 k(i, j) \sum_{n=0}^j \Upsilon(i, n) \Delta t \right] \times [k(i, j) \Upsilon(i, j)]^{0.5} \Delta t [M](i, j - 1) + \eta_4 T(i, j - 1) + \eta_5 \quad (\text{A14})$$

For the parameter estimation, no dynamics is applied to the parameter transition, as shown in Eq. (A13). However, the measurement equation for the parameter is a highly nonlinear one. The following derivative will be considered to analyze the observability.

$$\frac{\partial f_3}{\partial k} = \eta_3 \eta_1 \Delta t [M](i, j - 1) (\Phi_1 + \Phi_2) \quad (\text{A15})$$

where

$$\Phi_1 = \exp \left[\eta_2 k(i, j) \sum_{n=0}^j \Upsilon(i, n) \Delta t \right] [\Upsilon(i, j)]^{0.5} \frac{1}{2} k(i, j)^{-0.5} \quad (\text{A16})$$

$$\Phi_2 = \left\{ \exp \left[\eta_2 k(i, j) \sum_{n=0}^j \Upsilon(i, n) \Delta t \right] \eta_2 \sum_{n=0}^j \Upsilon(i, n) \Delta t \right\} [k(i, j) \Upsilon(i, j)]^{0.5}$$

For the units which are far away from the moving source, the term $\Upsilon(i, j)$ is almost zero. Then the following terms will be also close to zero:

$$\Phi_1 \approx 0, \quad \Phi_2 \approx 0, \quad \frac{\partial f_3}{\partial k} \approx 0 \quad (\text{A17})$$

This shows that the observability of the parameter estimation is also poor for those units away from the source.

References

- [1] P. Mills, Robotic UV curing for automotive exterior applications: a cost-effective and technically viable alternative for UV curing, in: North American Automotive UV Consortium Report, Stongsville, OH, USA, 2005.
- [2] T. Raith, M. Bischof, M. Deger, E. Gemmler, 3-D UV technology for OEM coatings, in: RadTech Report Article on Robotic UV Curing at Daimler Chrysler, Germany, 2001.
- [3] B. Croft, Use of infra-red and convection for drying and curing water-borne coatings, Product Finishing (London) 48 (October (9)) (1995) 7.
- [4] P. Dufour, D. Blanc, Y. Touré, P. Laurent, Infrared drying process of an experimental water painting: model predictive control, Drying Technology 22 (January/February(1–2)) (2004) 269–284.
- [5] A.G. Butkovskii, A.Y. Lerner, The optimal control of systems with distributed parameters, Automation and Remote Control 21 (1960) 472–477.
- [6] H. Yeh, J. Tou, Optimum control of a class of distributed parameter systems, IEEE Transactions on Automatic Control 12 (February (1)) (1967) 29–37.
- [7] M.A. Demetriou, O.V. Iftime, Finite horizon optimal control of switched distributed parameter systems with moving actuators, in: Proceedings of the 2005 American Control Conference, vol. 6, 2005, pp. 3912–3917.
- [8] M.A. Demetriou, A. Paskaleva, O. Vayena, H. Domanidis, Scanning actuator guidance scheme in a 1-D thermal manufacturing process, IEEE Transactions on Control Systems Technology 11 (September (5)) (2003).
- [9] J.P. Huissoon, D.L. Strauss, J.N. Rempel, S. Bedi, H.W. Kerr, Multi-variable control of robotic gas metal arc welding, Journal of Materials Processing Technology 43 (June (1)) (1994) 1–12.
- [10] P.D.A. Jones, S.R. Duncan, T. Rayment, P.S. Grant, Control of temperature profile for a spray deposition process, IEEE Transactions on Control Systems Technology 11 (September (5)) (2003) 656–667.
- [11] C. Domanidis, N. Fourligkas, Distributed parameter control of the heat source trajectory in thermal materials processing, Journal of Manufacturing Science and Engineering 118 (November (4)) (1996) 571–578.
- [12] F. Zeng, B. Ayalew, M. Omar, Robotic automotive paint curing using thermal signature feedback, Industrial Robot: An International Journal 36 (4) (2009) 389–395.
- [13] F. Zeng, B. Ayalew, M. Omar, Cure-feature based online trajectory generation in a robotic paint curing system, in: Proceedings of the 2009 American Control Conference, St. Louis, MO, USA, June 10–12, 2009, pp. 2006–2011.
- [14] D. Dochain, State and parameter estimation in chemical and biochemical processes: a tutorial, Journal of Process Control 13 (8) (2003) 801–818.
- [15] K.A. Soucy, B.R. Holt, Modeling, estimation and control of polymer composite processing, in: Proceedings of the 1990 American Control Conference, 1990, pp. 1650–1655.
- [16] R.D. Braatz, J.G. VanAntwerp, A.P. Featherstone, B.A. Ogunnaike, Cross-directional control of sheet and film processes, Automatica 43 (February (2)) (2007) 191–211.
- [17] I.I. Hussein, M.A. Demetriou, Estimation of distributed processes using mobile spatially distributed sensors, in: Proceedings of the 2007 American Control Conference, 2007, pp. 2756–2761.
- [18] I. Ashdown, Radiosity: A Programmer's Perspective, John Wiley and Sons, New York, NY, 1994.
- [19] M.F. Modest, Radiative Heat Transfer, McGraw Hill, New York, NY, 1993.
- [20] W. Hong, Y.T. Lee, H. Gong, Thermal analysis of layer formation in a stepless rapid prototyping process, Applied Thermal Engineering 24 (February (2–3)) (2004) 255–268.
- [21] M.D. Goodner, C.N. Bowman, Development of a comprehensive free radical photopolymerization model incorporating heat and mass transfer effects in thick films, Chemical Engineering Science 57 (March (5)) (2002) 887–900.
- [22] B.-S. Chiou, S.A. Khan, Real-time FTIR and in situ rheological studies on the UV curing kinetics of thiol-ene polymers, Macromolecules 30 (November (23)) (1997) 7322–7328.
- [23] T. Renault, A.A. Ogale, M.J. Drews, Cure monitoring of photosensitive resins by photo-dynamic mechanical analysis, Polymer Engineering and Science 36 (February (4)) (1996) 551–557.
- [24] J.M. Biernacki, F.C. Beall, Acoustic monitoring of cold-setting adhesive curing in wood laminates, International Journal of Adhesion and Adhesives 16 (3) (1996) 165–172.
- [25] Haykin, S. Simon, Kalman Filtering and Neural Networks, John Wiley and Sons, New York, NY, 2001.
- [26] E.A. Wan, A.T. Nelson, Neural dual extended Kalman filtering: applications in speech enhancement and monaural blind signal separation, in: Neural Networks for Signal Processing, VII. Proceedings of the 1997 IEEE Signal Processing Society Workshop, 1997, pp. 466–475.
- [27] G.-I. Eduardo, M.-R. Hiram, Fuzzy multivariable control of a class of a biotechnology process, in: Proceedings of the IEEE International Symposium on Industrial Electronics, 1999, pp. 419–424.
- [28] L.A. Iriarte, G.L.A. Mota, R. Tanscheit, M.M. Vellasco, J.M. Barreto, Fuzzy control of a multivariable nonlinear process, in: Proceedings of the Eighth International Fuzzy Systems Association World Congress, vol. 2, 1999, pp. 660–664.
- [29] C.-H. Tsai, K.-H. Hou, H.-T. Chuang, Fuzzy control of pulsed GTA welds by using real-time root bead image feedback, Journal of Materials Processing Technology 176 (June (1–3)) (2006) 158–167.